

Spiral-Bevel Geometry and Gear Train Precision

Faydor L. Litvin* and John J. Coy†

Spiral-bevel gears have widespread applications in the transmission systems of helicopters, airplanes, trucks, automobiles and many other machines. Some of the major requirements in almost all the fields of application for transmissions are (1) improved life and reliability, (2) reduction in overall weight (i.e., a larger power-to-weight ratio) without compromising the strength and efficiency during the service life, and (3) reduction in the transmission noise.

Spiral-bevel gears used in practice are normally generated with approximately conjugate tooth surfaces by using special machine and tool settings. Therefore, designers and researchers cannot solve the Hertzian contact stress problem and define the dynamic capacity and contact fatigue life (ref. 1) until these settings are calculated. The geometry of gear tooth surfaces is very complicated and the determination of principal curvatures and principal directions of tooth surfaces necessary for calculating the Hertz stress is a very hard problem.

Baxter (refs. 2 and 3), Litvin (refs. 4 to 7), Litvin and Gutman (refs. 8 and 9) and Wildhaber (ref. 10) completed works dealing with the theory of gearings as well as with the theory of spiral bevel gears. Coy, Townsend, and Zaretsky (ref. 1), Coy, Rohn, and Loewenthal (ref. 11) completed work dealing with dynamic capacity and surface fatigue life of gears. Townsend, Coy, and Hatvani (ref. 12) analyzed failures of a helicopter transmission.

In this paper a novel approach to the study of the geometry of spiral bevel gears and to their rational design is proposed. The nonconjugate tooth surfaces of spiral-bevel gears are, in theory, replaced (or approximated) by conjugated tooth surfaces. These surfaces can be generated (1) by two conical surfaces rigidly connected with each other and in linear tangency along a common generatrix of tool cones, and (2) by a conical surface and a surface of revolution in linear tangency along a circle.

We can imagine that four surfaces are in mesh: two of them are tool surfaces Σ_F and Σ_K ; and two are gear tooth surfaces Σ_1 and Σ_2 . Surfaces Σ_F and Σ_1 are in linear contact, and contact lines of different form appear on the contacting surfaces in the process of meshing of the generating and the generated surfaces. The same can be said about the contact of surfaces Σ_K and Σ_2 . Surfaces Σ_F and Σ_K are rigidly connected and move in the process of meshing as one body. Surfaces Σ_1 and Σ_2 are in point contact and the point of their contact moves along these surfaces in the process of meshing. Surfaces Σ_1 and Σ_2 are hypothetical conjugate tooth surfaces which approximate the actual nonconjugate tooth surfaces.

The determination of surface principal curvatures and directions is a complicated problem. Therefore, a new approach to the solution of these is proposed in this presentation. In this approach direct relationships between the principal curvatures and directions of the tool surface and those of the generated gear surface are obtained. Therefore, the principal curvatures and directions of gear-tooth surface are obtained without using the complicated equations of these surfaces. This makes it easier to apply previously worked out methods for calculating life and reliability for spur and helical gears and traction-drive contacts to the spiral-bevel gear problem.

A general theory of the train kinematical errors exerted by manufacturing and assembly errors is discussed. Two methods for the determination of the train kinematical errors can be worked out: (1) with the aid of a computer, and (2) with an approximate method. Results from noise and vibration measurement conducted on a helicopter transmission are used to illustrate the principals contained in the theory of kinematical errors.

*University of Illinois at Chicago Circle.

†NASA Lewis Research Center.

Spiral-Bevel Geometry

Figure 1 shows the generating gear g and the member-spiral bevel gear 2 in mesh by cutting. The generating gear rotates about the axis x_f , and the member-gear rotates about the axis z_2 . Axes x_f and z_2 form an angle $90^\circ + (\gamma_2 - \Delta_2)$, where γ_2 is the pitch cone angle and Δ_2 is the addendum angle Δ_2 of the member gear 2.

Figure 2 shows the generating gear g and the pinion in mesh by cutting. The axes of rotation x_f and z_1 form an angle $90^\circ - (\gamma_1 - \Delta_1)$, where γ_1 is the pitch-cone angle and Δ_1 is the addendum angle of the pinion 1. It is assumed that gears 1 and 2 rotate in the train about perpendicular axes.

Surfaces of gears 1 and 2 can be generated as conjugated ones if axis z (fig. 3) is an instantaneous axis of rotation in relative motion for all four gears (for gears 1 and 2 and two generating gears). This requirement cannot be fulfilled for spiral bevel gears because the axes of rotation of the generating gears do not coincide with each other but form an angle $\Delta_1 + \Delta_2$ (fig. 3). Therefore, special machine settings by pinion 1 cutting are applied (fig. 2): axes of rotation x_f and z_1 do not intersect with each other and are dislocated by ΔL_1 and ΔE_1 in two perpendicular directions (ΔE_1 is not shown in fig. 2).

The novel approach to the study of the geometry of spiral-bevel gears is based on the substitution of nonconjugated tooth surfaces by conjugated ones, which can be realized in the following two ways or versions. It is well known that the generating surface for spiral-bevel gears is conical (fig. 4). The first version of spiral-bevel geometry is based on the following propositions: (a) two generating conical surfaces are in linear tangency along a common generatrix of both cones (fig. 5); (b) it can be imagined that two generating surfaces are rigidly connected with each other and rotate as one body by gear generation. The surfaces of the generated gears will therefore be in point tangency. The point of contact of the gear surfaces in mesh moves along the common generatrix of the tool cones. This imaginary way of gear meshing results in elliptical-shaped Hertzian contacts which move across the tooth surfaces in the profile direction.

The second version of the spiral-bevel geometry is based on these propositions: (1) One of the generating surfaces is conical, and the other is a surface of revolution (fig.6); (2) both generating surfaces are in linear tangency along a circle of radius r_d ; (3) it is assumed that both generating surfaces are rigidly connected and rotate as one body by gear generation.

Surfaces of generated gears with geometry II will also be in point contact. The point of contact between the gear surfaces in mesh moves along the circle of radius r_d (fig. 6). This second version of gear generation provides that motion of the Hertzian ellipse contact will be along the gear tooth surface in the longitudinal direction. The advantages of spiral-bevel geometry II that are possible to achieve are improved conditions of lubrication and increased contact ratio.

Figure 7 shows a generating surface Σ_d which is covered with lines of contact. The generating and generated surfaces are in instantaneous contact at one of these lines. The point of instantaneous

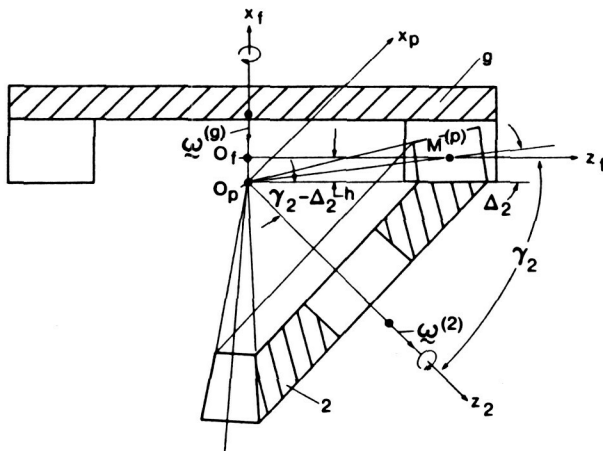


Figure 1. - Generating gear and member gear.

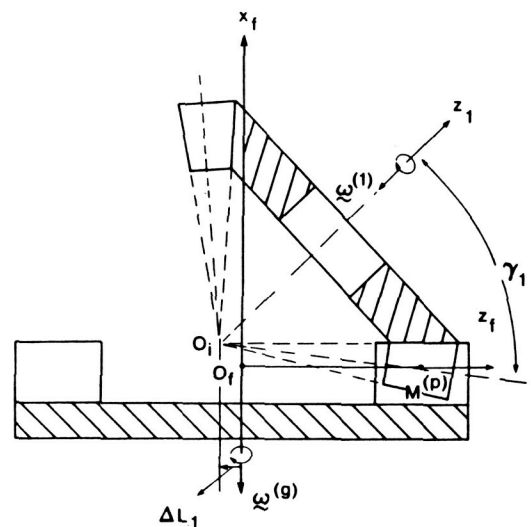


Figure 2. - Generating gear and pinion.

contact of gear surfaces is the point of intersection of the corresponding contact line with the tool cone generatrix (fig. 7). This generatrix is the line of contact of two tool cones for gears with the geometry I. An analogous picture pertains for gear geometry II, but the contact point between the gear surfaces is the point of intersection of the instantaneous contact line with the circle of radius r_d , which is the line of tangency of the two tool cones (fig. 6).

The analytical representation of the gear surface contact condition is based on the proposition that radii-vectors and unit normals of surfaces coincide at the contact point, M (fig. 8).

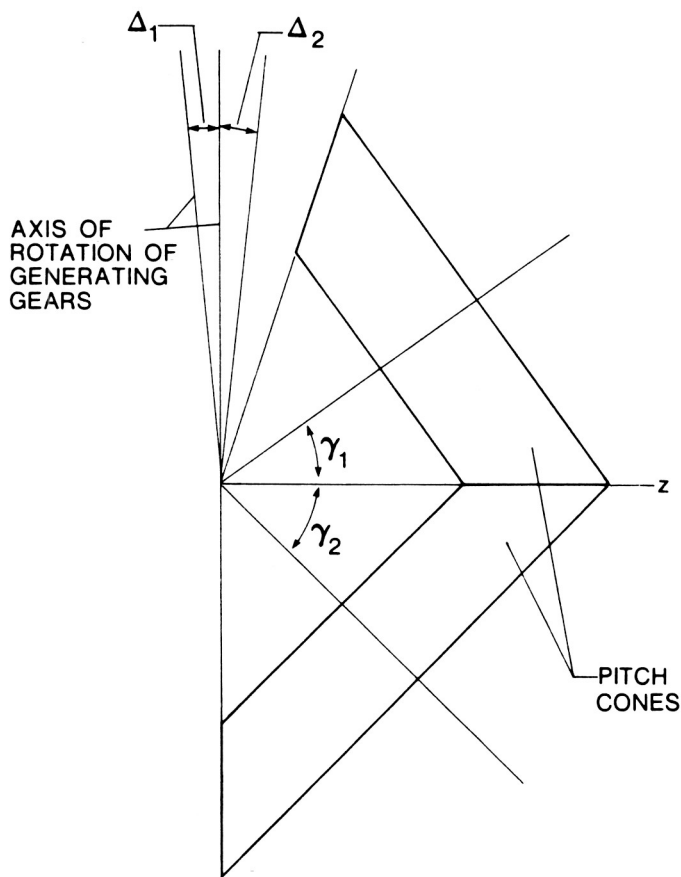


Figure 3. - Axes of rotation of generating gears and member gears.

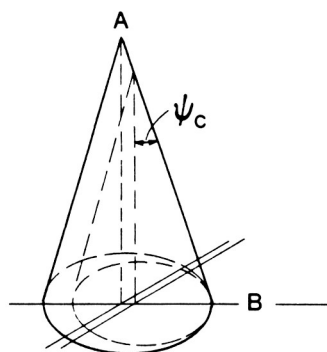


Figure 5. - Generating surfaces for geometry I.

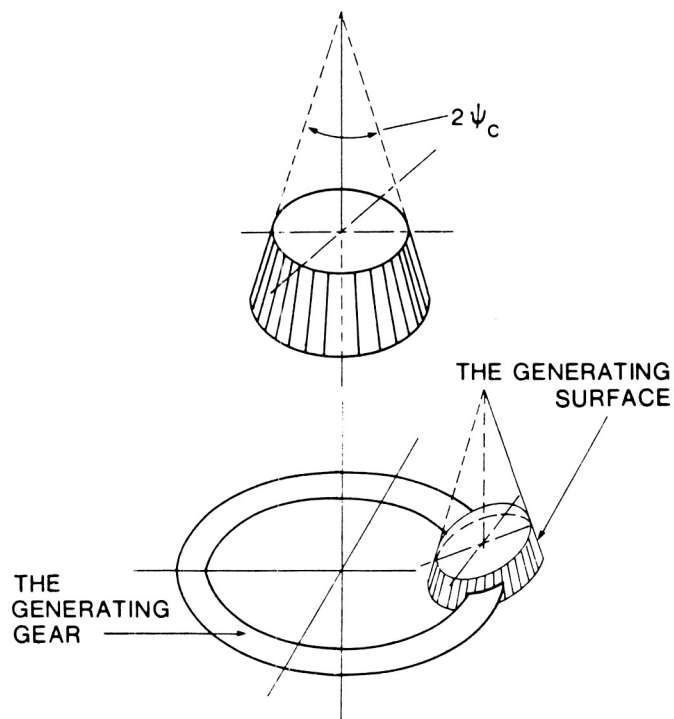


Figure 4. - Tool cone and generating gear.

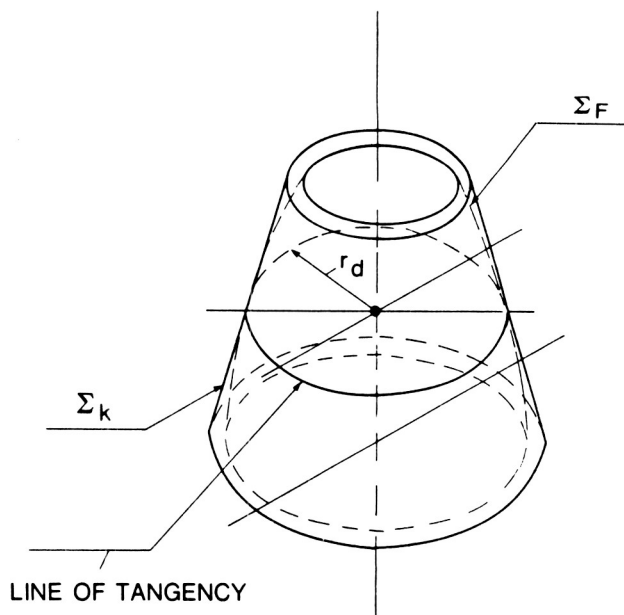


Figure 6. - Generating surfaces for geometry II.

Because of elasticity of gear surfaces, their contact under a load is spread over an area (fig. 9) which, when projected on the tangent plane, is an ellipse. Figure 10 shows how the bearing contact is formed for gears with geometry I (fig. 10(a)) and for gears with geometry II (fig. 10(b)). The location of the bearing contact on the tooth surface depends on the direction of motion of the elliptical spot over the tooth surface.

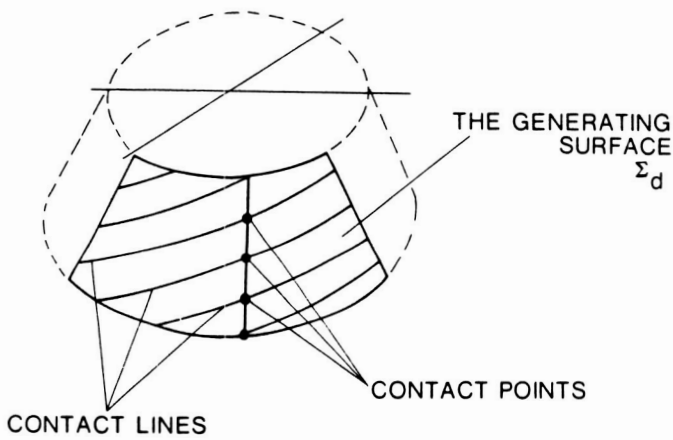


Figure 7. - Contact lines and contact points on generating surface Σ_d .

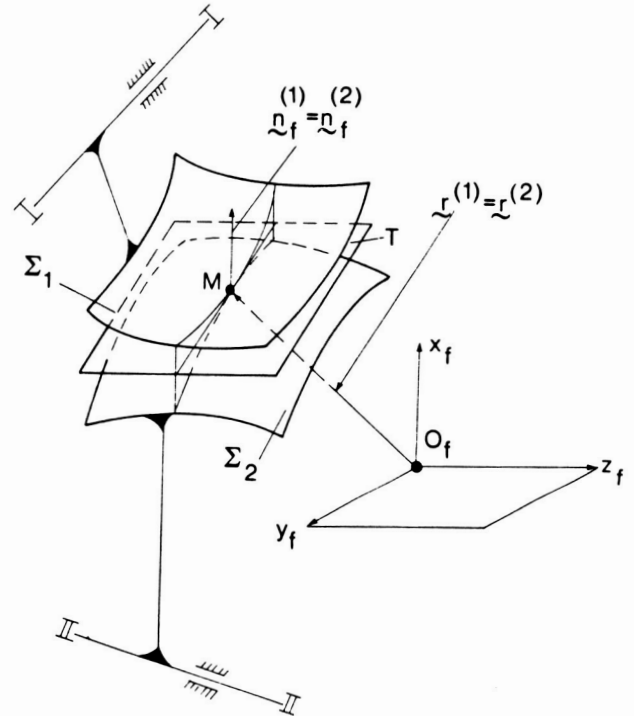


Figure 8. - Gear tooth surfaces at contact.

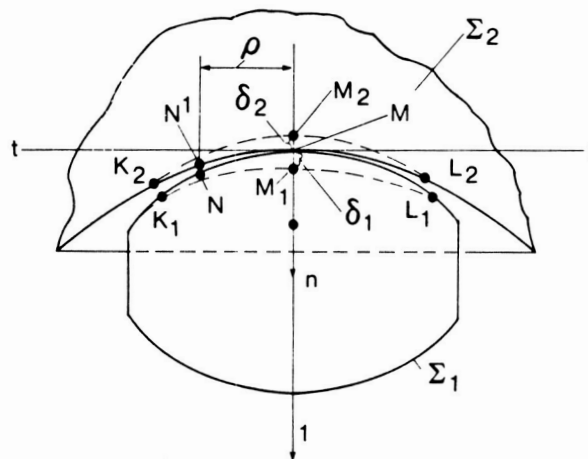


Figure 9. - Deformation of two contacting surfaces.

Method of Calculation of Dynamic Capacity and Surface Fatigue Life of Spiral Bevel Gears

In reference 1 a method of adapting the Lundberg-Palmgren method of life analysis for rolling-element bearings was applied to spur and helical gears. The method has also been applied to life analysis of traction drives (ref. 11). An update of the method applied to spur gears, with applications for various gearing arrangements, is presented in another paper in this symposium.

In the life analysis theory the important parameters are number of stress cycles, η , magnitude of critical stress, τ , amount of stressed volume, V , and depth below the surface at which the critical stress occurs, z . For spiral bevel gears, the stressed volume is taken as

$$V \propto wzl \quad (1)$$

where l is the length of the contact path which is traversed during one tooth mesh cycle and the semi-width of the contact path is designated w .

The probability of survival, S , for a tooth contact is given by the following expression:

$$\log \frac{1}{S} \propto \frac{\tau^c \eta^e V}{z^h} \quad (2)$$

This relation is consistent with experimental observations in the case of fatigue. The formula reflects the known fact that the more localized the stress is in the material (less stressed volume), the greater is the endurance. This is because, on a statistical basis, there is less likelihood of a fatigue nucleation site being coincident with a condition of high stress. Conversely, there is a greater probability of a crack forming in the zone of maximum critical stress, because the material is more rapidly cycled toward failure in that region. Hence the depth to the critical stress, as well as the magnitude of the stress is important, and with each stress cycle the probability of failure increases.

The number of stress cycles endured with 90 percent reliability is given by the following equation (ref. 11):

$$\eta = \left(\frac{Kz^h}{\tau^c V} \right)^{1/e} \quad (3)$$

Based on life testing of air-melted steel rolling-element bearings, the following values are valid for equation (3): $K = 1.43 \times 10^{95}$ (SI units), 3.58×10^{56} (English units); $h = 7/3$; $c = 31/3$; and $e = 10/9$ (point contact), $3/2$ (line contact) (ref. 11).

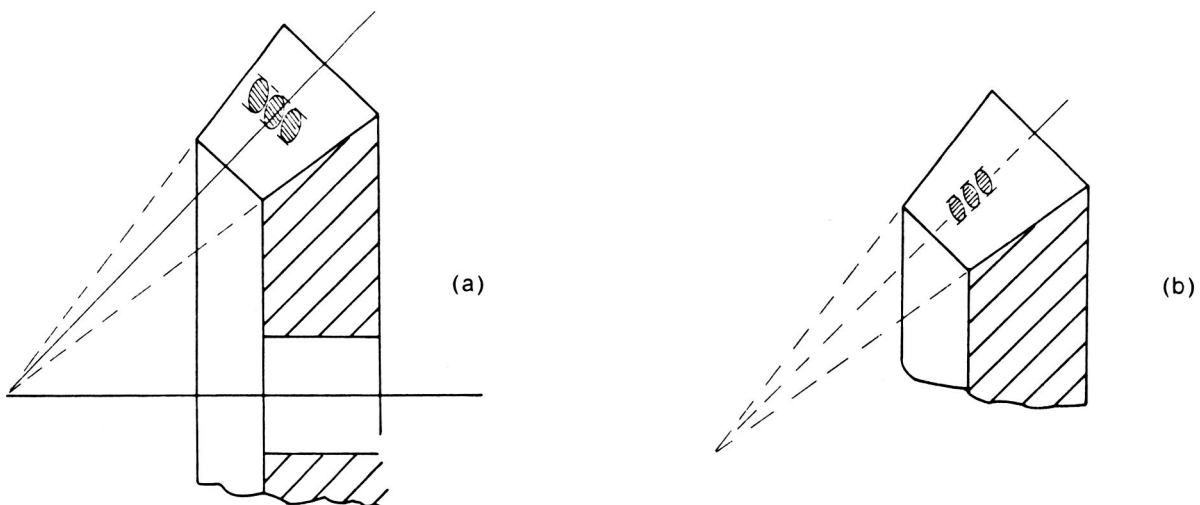


Figure 10. - Formation of bearing contact.

From the probability theory the life, L , of a gear with N teeth then is obtained by the equation

$$\left(\frac{1}{L}\right)^e = N \left(\frac{1}{\eta}\right)^e \quad (4)$$

The foregoing has been a brief summary of how the gear life analysis originally presented in reference 10 may be applied to spiral-bevel gears. All of the approximations, service life factors and lubricant-condition-related life-modifying factors that pertain to spur and helical gears will also have counterpart effects for spiral-bevel gears. These factors are discussed in reference 11.

Gear Train Precision

Angles of rotation φ_2 and φ_1 of a pair of gears are related by a linear function only for an ideal train. The difference

$$\varphi_2(\varphi_1) - \varphi_2^0(\varphi_1) = \Delta\varphi_2(\varphi_1) \quad (5)$$

represents a function of kinematical errors induced by errors of manufacturing and assembly. Here, $\varphi_2^0(\varphi_1)$ is the theoretical function, and $\varphi_2(\varphi_1)$ is the real function.

The function $\Delta\varphi_2(\varphi_1)$ of kinematical errors may be determined in the following two ways:

The first method is based on the investigation of the meshing of gear surfaces generated and assembled with some errors. The basic principle of such an investigation is the requirement of equality of radii vectors and unit normals of contacting surfaces (fig. 8). The determination of gear-train kinematical errors with such a method is a computer problem.

The second method is based on the following suggestions (fig. 11): Suppose that, because of errors of manufacturing and assembly, the expected contact points $M^{(1)}$ and $M^{(2)}$ do not coincide with each other and that between surfaces Σ_1 and Σ_2 there occurs clearance or interference. To bring both surfaces into contact, it is necessary and sufficient to rotate the driven gear 2 about the axis II-II by some small angle $\Delta\varphi_2$, the magnitude of which depends on the magnitude of clearance or

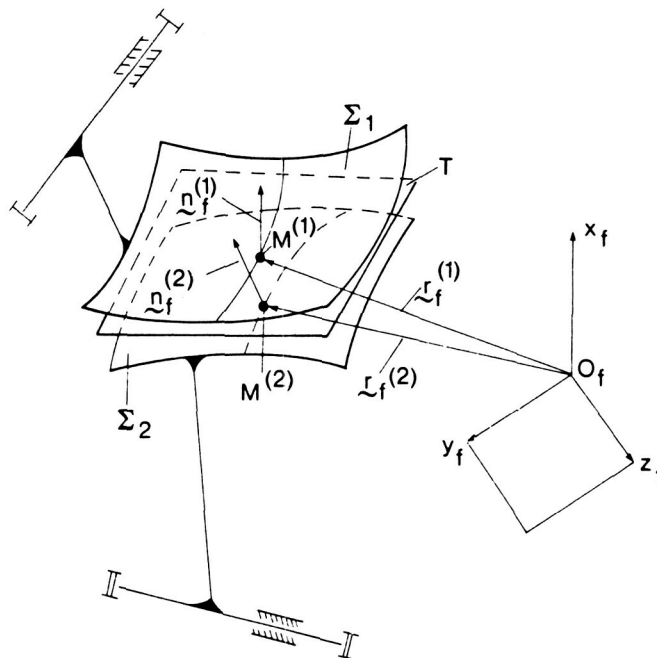


Figure 11. - Tooth surfaces with clearance induced by errors.

interference induced by errors of manufacturing and assembly. Equations relating kinematical errors with errors of manufacturing and assembly have been developed by Litvin (refs. 4 and 5).

Figure 12 shows kinematical errors $\Delta\phi_2(\phi_1)$ represented by equation (5). Figure 13 shows two types of the function $\Delta\phi_2(\phi_1)$. The first one (fig. 13(a)) corresponds to the case when the gear axis does not coincide with the axis of rotation and rotates about it in the process of meshing. The typical example of such errors is the gear eccentricity. The second type of kinematical errors of a train with spiral-bevel gears and hypoid gears is the result of the approximate way of gear generation (fig. 13(b)).

Figure 14 shows a case when a gear axis, z_1 , forms an angle $\Delta\delta$ with the axis of rotation, z , and the shortest distance between z_1 and z is the rotated vector Δe . With $\Delta\delta=0$ the vector Δe represents the vector of gear eccentricity.

Figure 15 shows two spur involute gears with vectors of eccentricity Δe_1 and Δe_2 . Gear axis of rotation are $O^{(1)}$ and $O^{(2)}$, geometric centers of gears are O_1 and O_2 . These centers rotate about $O^{(1)}$ and $O^{(2)}$ as shown in figure 16. The eccentricity of a spur gear exerts a harmonic function (fig. 17) of kinematical errors $\Delta\theta_1(\phi_i)$, the period of which coincides with the period of a complete revolution of the considered gear. The distribution of this function in positive and negative areas depends on the location of the vector eccentricity.

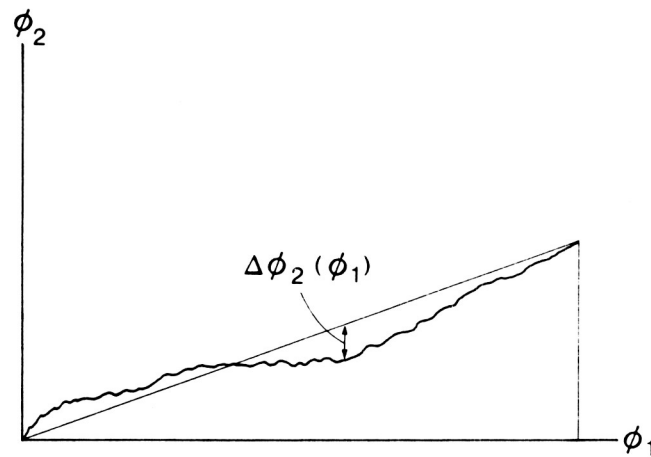


Figure 12. - Kinematic error functions.

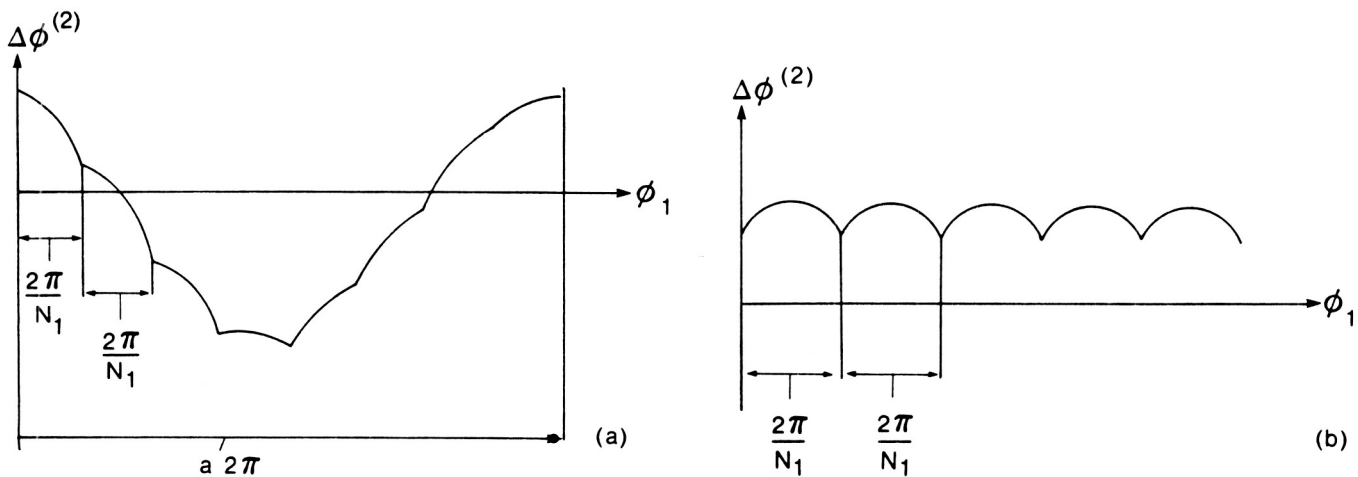


Figure 13. - Two types of kinematic functions.

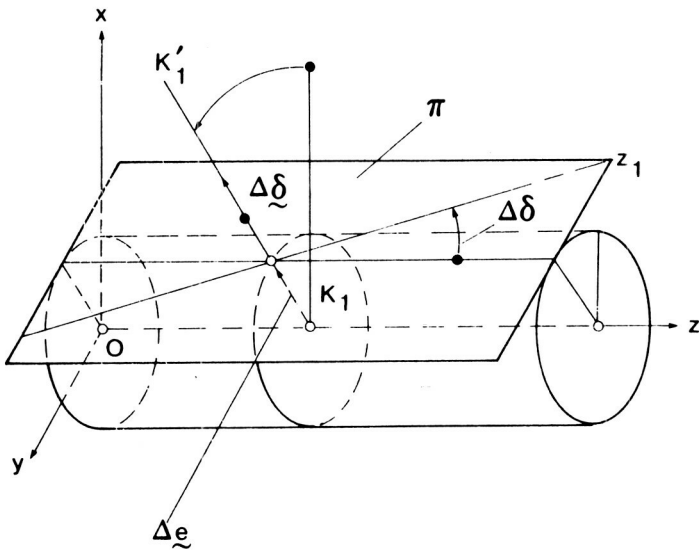


Figure 14. - Crossing of gear axis and rotation axis.

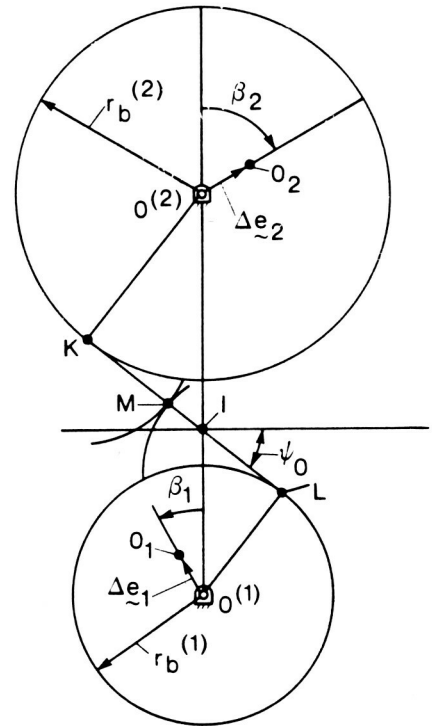


Figure 15. - Eccentricity of spur gears.

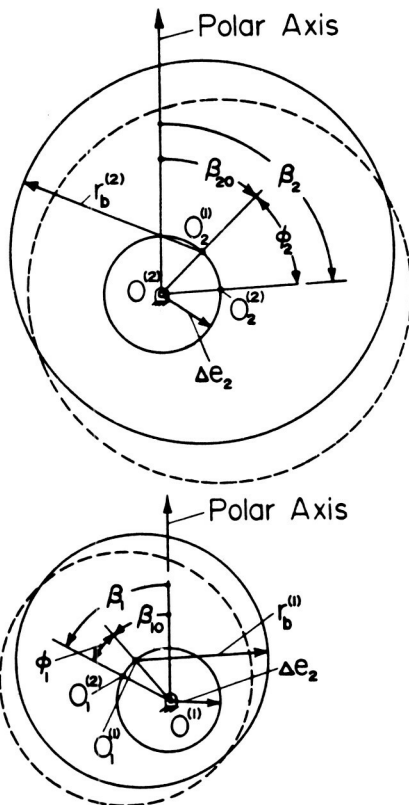


Figure 16. - Eccentric base circles.

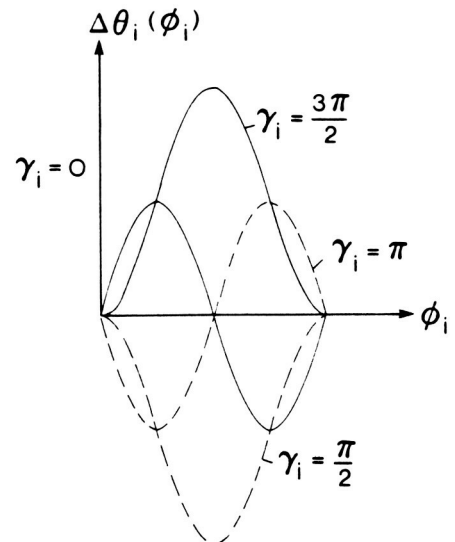


Figure 17. - Distribution of kinematic errors by eccentricity.

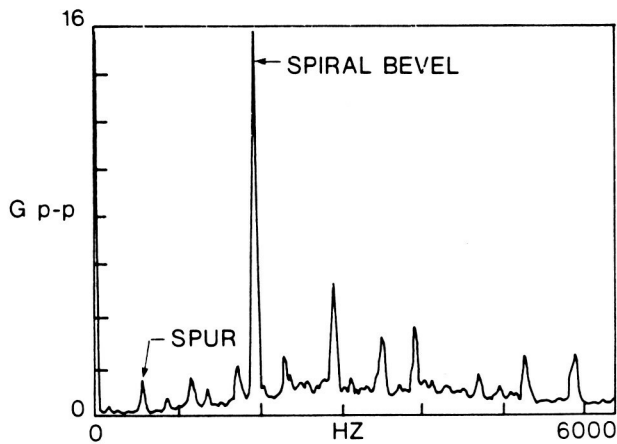


Figure 18. - Baseband frequency spectrum showing spiral bevel amplitude compared with spur.

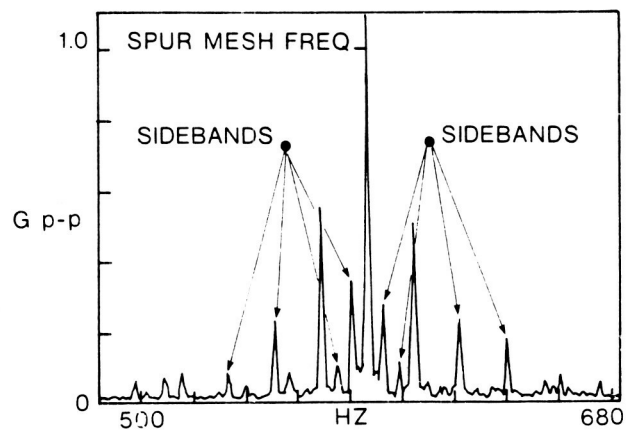


Figure 19. - Narrowband frequency spectrum showing sidebands around the spur mesh frequency.

Gear Train Vibration and Noise Measurement

To illustrate the principles discussed on the subject of gear-train precision, figures 18 and 19 are used. These figures show some frequency spectrum measurements made on a helicopter transmission running in a test stand (ref. 12). The transmission had a spiral-bevel input stage with 19 teeth on the pinion and 71 teeth on the gear. The pinion was turning at 6200 rpm and the output shaft at 355.5 rpm. The output stage was a spur planetary arrangement with a 27-tooth sun, 3 planet gears, each with 35 teeth, and a 99-tooth ring gear which was splined to the transmission housing. An accelerometer was mounted on the case immediately outside the spline.

Figure 18 shows a broadband frequency spectrum measurement of the vibration signal. The spur mesh frequency was 583 Hz, and the spiral bevel mesh frequency was 1963 Hz. The spiral bevel vibration signature was much stronger than the spur signature. This indicates that the meshing accuracy according to figure 13(b) was better for the spur mesh than for the spiral-bevel mesh. There are also other peaks in the spectrum at multiples of the fundamental frequencies of 1963 and 583 Hz. These other peaks are the higher harmonics due to the noise and vibration pulsations as the teeth mesh being different from the pure sinusoidal shape, as shown in figure 17.

Figure 19 shows an expanded region of the autospectrum plot given in figure 18. This figure shows many peaks which are symmetrically located about the spur gear mesh fundamental frequency peak at 583 Hz. These peaks locate the sideband frequencies which are due to sources of modulation in the time-dependent vibration waveform. Each source of modulation may produce one pair of sidebands if it is a harmonic modulator. If nonharmonic, the sidebands will repeat many times, as is the case in figure 19.

In this particular example, there are three major causes of modulation: (1) the planet gears passing the stationary accelerometer at approximately 18 Hz; (2) the planet gears rotational speed of 16 Hz; and (3) the planet carrier turning at the output shaft speed of 6 Hz. The misalignments and eccentricities associated with the rotational frequencies of the mentioned gear components cause these modulation sidebands to appear, as discussed in the previous section.

Conclusions

Two types of spiral-bevel geometry for a simplified study and investigation of such gears were described. The line of action and bearing contact for gears of both types of geometry were determined. A method for calculating the expected service life for pitting fatigue of the spiral-bevel gear teeth was given.

Two methods for the determination of kinematical errors induced by errors of manufacturing and assembly were proposed. The first is an exact computerized method, the second is an approximate one but one which allowed the analytical relations between source errors and resulting kinematical errors to be written. Results of noise and vibration measurements on a helicopter transmission were shown to illustrate the principles contained in the theory of kinematical errors.

References

1. Coy, J. J.; Townsend, D. P.; and Zaretsky, E. V.: Dynamic Capacity and Surface Fatigue Life for Spur and Helical Gears. *J. Lubr. Technol.*, vol. 98, no. 2, April 1976, pp. 267-276.
2. Baxter, M.: Second-Order Surface Generation. *Ind. Math.*, vol. 23, pt. 2, 1973, pp. 85-106.
3. Baxter, M.: Effect of Misalignment on Tooth Action of Bevel and Hypoid Gears. ASME Paper No. 61-MD-20.
4. Litvin, F.: *Theory of Gearing*, 2nd. Ed., Nauka, 1968 (in Russian).
5. Litvin, F.: Die Beziehungen zwischen den Krümmungen der Zahnoberflächen bei räumlichen Verzahnungen. *ZAMM*, 49 (1969), Heft 11, Seite 685-690.
6. Litvin, F.: The Synthesis of Approximate Meshing for Spatial Gears. *J. Mechanisms*, vol. 4, 1969, Pergamon Press, pp. 187-191.
7. Litvin, F.: An Analysis of Undercut Conditions and of Appearance of Contact Lines Envelope Conditions of Gears. *J. Mech. Des.*, July 1978, pp. 423-432.
8. Litvin, F.; and Gutman, Ye.: Methods of Synthesis and Analysis for Hypoid Gear Drives of "Formate" and "Helixform," Pts. 1-3, *J. Mech. Des.*, vol. 103, Jan. 1981, pp. 83-113.
9. Litvin, F.; and Gutman, Ye.: A Method of Local Synthesis of Gears Grounded on the Connections Between the Principal and Geodetic Curvatures of Surfaces. *J. Mech. Des.*, vol. 103, 1981, pp. 114-125.
10. Wildhaber, E.: Surface Curvature—A Tool for Engineers. *Ind. Math.*, vol. 5, 1954, pp. 31-116.
11. Coy, J. J.; Rohn, D. A.; and Loewenthal, S. H.: Life Analysis of Multiroller Planetary Traction Drive. NASA TP-1710, April 1981.
12. Townsend, D. P.; Coy, J. J.; and Hatvani, B. R.: OH-58 Helicopter Transmission Failure Analysis. NASA TM X-71867, Jan. 1976.